

# The stability of the optical flux variation gradient for 3C 120

Michael Ramolla<sup>1</sup>, Francisco Pozo Nuñez<sup>1</sup>, Christian Westhues<sup>1</sup>, Martin Haas<sup>1</sup>, and Rolf Chini<sup>1,2</sup>

<sup>1</sup> Astronomisches Institut, Ruhr-Universität Bochum, Universitätsstraße 150, 44801 Bochum, Germany  
e-mail: ramolla@astro.rub.de

<sup>2</sup> Instituto de Astronomía, Universidad Católica del Norte, Avenida Angamos 0610, Casilla 1280 Antofagasta, Chile

Received –; accepted –

## ABSTRACT

New  $B$ - and  $V$ -band monitoring in 2014 – 2015 reveals that the Seyfert 1 Galaxy, 3C 120, has brightened by a magnitude of 1.4, compared to our campaign that took place in 2009 – 2010. This allowed us to check for the debated luminosity and time-dependent color variations claimed for SDSS quasars. For our 3C 120 data, we find that the  $B/V$  flux ratio of the variable component in the bright epoch is indistinguishable from the faint one. We do not find any color variability on different timescales ranging from about 1 to 1800 days. We suggest that the luminosity and time-dependent color variability is an artifact caused by analyzing the data in magnitudes instead of fluxes. The flux variation gradients of both epochs yield consistent estimates of the host galaxy contribution to our  $7''.5$  aperture. These results confirm that the optical flux variation gradient method works well for Seyfert galaxies.

**Key words.** galaxies: active – galaxies: Seyfert – galaxies: nuclei –

## 1. Introduction

The UV to optical color ratio of the total AGN, measured in magnitude units, becomes bluer as the AGN brightens (e.g. Meusinger et al. 2011). Some studies attribute this change in color to the spectral hardening of the variable component (Giveon et al. 1999; Wilhite et al. 2005; Wamsteker et al. 1990; Webb & Malkan 2000). However, there is ample evidence to suggest that the color of the variable component stays constant and that the corresponding flux variation gradient is offset from the origin of the flux–flux diagram (Choloniewski 1981; Winkler et al. 1992; Winkler 1997; Paltani & Walter 1996; Sakata et al. 2010). In this case, the ‘bluer when brighter’ total observed fluxes, which are measured in a finite aperture, are explained by the superimposition of a constant red host galaxy (including non-varying emission lines) and a varying blue AGN. Even if the measured host contribution is small, compared to the required offset of the flux variation gradient (FVG), there is no significant curvature seen in the flux–flux diagrams (Sakata et al. 2011).

The constancy of the optical colors of the variable component is physically plausible if the variable emission has a hot thermal origin, as expected for an accretion disk (AD). In this case, fluxes in the optical range lie on the Rayleigh-Jeans tail, and they scale almost linearly with temperature.

Recently, Sun et al. (2014) report time-dependent  $g/r$  color variability of the SDSS Stripe 82 quasar sample. A blue color at variations inside  $<30$  days (with smaller amplitudes) gradually changes to redder colors on larger timescales  $>1000$  days (and larger amplitudes). Furthermore, Sun et al. (2014) claim that the FVG method lacks rigor and is, therefore, not valid. Consequently, one also expects to find similar behavior for Seyfert galaxies, the less luminous siblings of quasars.

Using data from 2009 – 2010, Pozo Nuñez et al. (2012) performed  $B$ -,  $V$ -band monitoring of the Seyfert 1 Galaxy 3C 120 including dense daily observations over a period of five months.

Here we report new  $B$ -,  $V$ -band results from a six-month monitoring project in 2014 and 2015. The total brightening (by about 1.4 mag) and the dense time-sampling of observations allow us to check whether or not brightness and time-dependent color variations are present.

## 2. Observations and data reduction

The new photometric data at Johnson  $B$  and  $V$  was observed between 27 August 2014 and 3 March 2015 at the Universitätssternwarte Bochum, near Cerro Armazones. We combined the RoBoTT telescope data (Pozo Nuñez et al. 2012) with new data from the BEST II (Kabath et al. 2009).

All data has been corrected for the latest revision of galactic foreground extinction<sup>1</sup> by Schlafly & Finkbeiner (2011) and the corresponding lightcurves are displayed in Figs.1 and 2.

## 3. Results

### 3.1. Flux-flux diagrams

Total  $B$ - versus  $V$ -band fluxes for the two epochs are shown in Fig. 3, with one that had low luminosity in 2009–2010 and one that had high luminosity in 2014–2015. Between the two epochs, the AGN luminosity increased by a magnitude of about 1.4 in both filters. The slope of AGN variability is well matched by a linear relation with  $\Gamma_{BV} = 0.979 \pm 0.005$ .

We consider the host colors of 3C 120 by Sakata et al. (2010) in a  $8''.3$  aperture, corrected for galactic foreground extinction (Schlafly & Finkbeiner 2011). Assuming that these will be similar when looked at in our  $7''.5$  aperture, this allows us to compute our own host fluxes by measuring the center of gravity of the area that is encased by the cone of AGN slope  $\Gamma_{BV}$ -fitting uncertainties and Sakata’s host color  $\Gamma_{BV,Host}$  (inside the red circle of

<sup>1</sup>  $A_{\lambda}^B = 1.079, A_{\lambda}^V = 0.816$

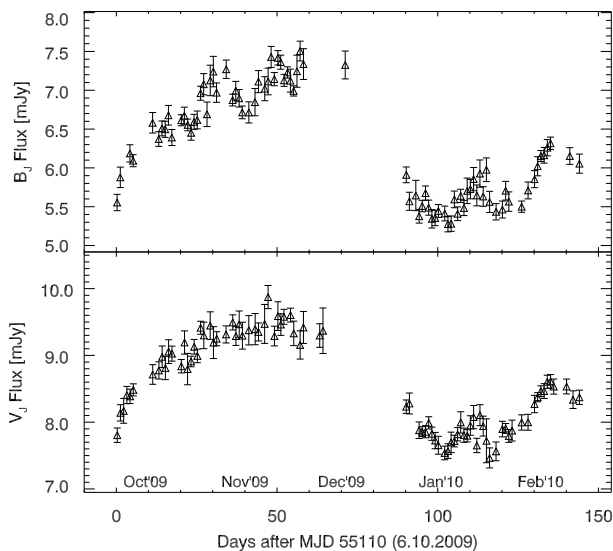


**Fig. 1.** Lightcurves in the 2009 – 2010 epoch obtained with the RoBoTT telescope. All fluxes are corrected for galactic foreground extinction.

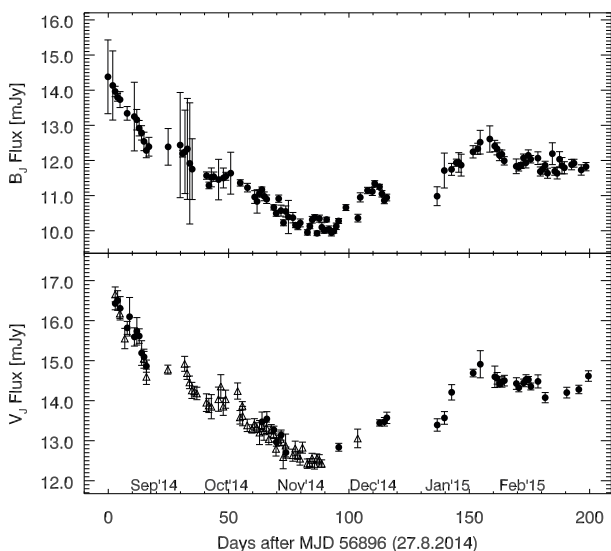


**Fig. 2.** Combined lightcurves in the 2014 – 2015 epoch, obtained with two different telescopes. Filled circles correspond to BEST II, while open triangles represent the RoBoTT observations. All fluxes are corrected for galactic foreground extinction.

Fig. 3). The results for the  $B$ - and  $V$ -band host fluxes (Table 1) agree well with the values of Sakata. We also fit the slopes of the individual epochs of 2009–2010 and 2014–2014 separately. For both epochs the slope is slightly flatter than the combined one, but they agree within the errors.

The offset of the combined slope (2009 – 2015) to the individual epoch slopes could imply that the short-term variability is redder than the long-term one. A more likely physical explanation, however, is based on the systematically different instrumental point spread functions (PSF). The PSF of the RoBoTT is slightly larger than that of the BEST II. The host also has a different spatial flux distribution at  $B$  and  $V$ . This leads to a larger host galaxy contribution in the 2009 – 2010 light curves, and the host galaxy contribution is larger in  $V$  than in  $B$ . In the net effect, compared to the 2014 – 2015 data, the 2009 – 2010 data appear slightly shifted in the FVG diagram toward the right, resulting in a marginally steeper overall  $\Gamma_{BV}$ . We believe that these neg-

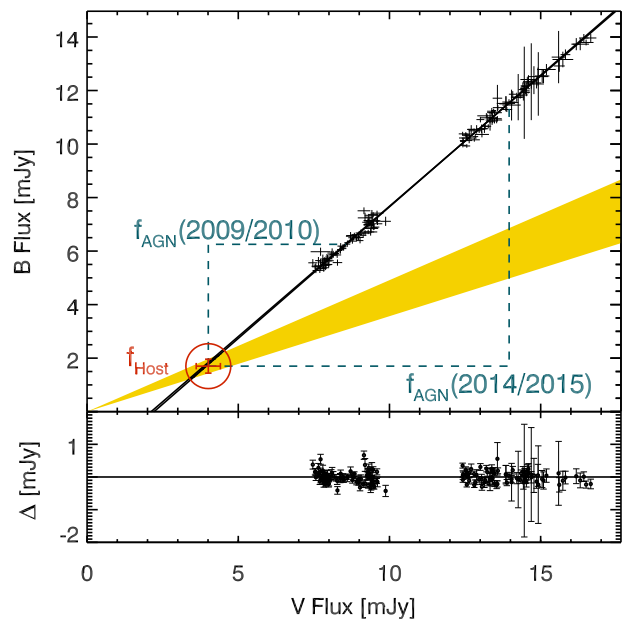


**Fig. 3.**  $B$  versus  $V$  flux variations of 3C 120 in the  $7''.5$  aperture. Each measurement is drawn as a thin cross in which the line length corresponds to the photometric uncertainties in the respective filters. The yellow filled area is the assumed host color  $\Gamma_{BV,Host}$ , drawn to cover  $B = (1.70 \pm 0.27)$  mJy and  $V = (4.01 \pm 0.62)$  mJy host fluxes, as determined by Sakata et al. (2010) in an  $8''.3$  aperture. Our host flux estimate is the datapoint in the red circle. All data from 2009 until 2015 was used to determine the AGN slope. The black continuous line covers the upper and lower standard deviations in the AGN slope, given by the OLS bisector fit.

**Table 1.** Results of the FVG analysis, separated into epochs and filter sets  $B$  and  $V$ . All fluxes in mJy are corrected for galactic foreground extinction as determined by Schlafly & Finkbeiner (2011). The host fluxes may also contain contributions from non-variable, narrow and broad emission lines.

Epoch, Filter	$f_{Host}$	$f_{AGN}$	$\Gamma_{AGN}$
	(mJy)		
2009 – 2015, $B$	$1.69 \pm 0.28$	–	$0.979 \pm 0.005$
2009 – 2015, $V$	$3.89 \pm 0.29$	–	“
2009 – 2010, $B$	$1.59 \pm 0.26$	$4.66 \pm 0.72$	$0.963 \pm 0.036$
2009 – 2010, $V$	$3.72 \pm 0.32$	$4.84 \pm 0.76$	“
2014 – 2015, $B$	$1.51 \pm 0.26$	$10.03 \pm 1.08$	$0.959 \pm 0.015$
2014 – 2015, $V$	$3.48 \pm 0.31$	$10.47 \pm 1.14$	“

ligible effects do not alter the basic results and conclusions on the stability of the FVG method because for all three data sets (2009 – 2010, 2014 – 2015, and 2009 – 2015) the host galaxy contribution is in excellent agreement within the errors. In  $B$ -band we measure a minimum  $f_{B,AGN} = 3.59$  mJy and a maximum of  $f_{B,AGN} = 12.69$  mJy. Correspondingly, the increase in  $V$  ranges from a minimum of  $f_{V,AGN} = 3.57$  mJy to a maximum of  $f_{V,AGN} = 12.76$  mJy.

### 3.2. Search for timescale-dependent AGN colors

The aim of this section is to investigate potential, timescale-dependent variability that has recently been observed by Sun et al. (2014) in a sample of Stripe 82 SDSS quasars. The

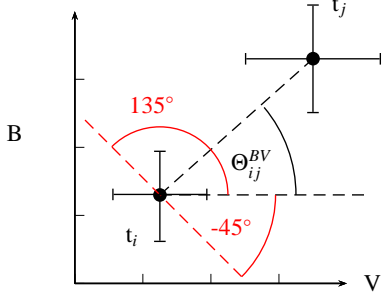


**Fig. 4.** Scheme of the color slope  $\Theta_{ij}^{BV}$  in the  $B$ - to  $V$ -band flux plane between two measurements  $t_i$  and  $t_j$  with photometric uncertainties. If  $\Theta$  falls below  $-45^\circ$  or above  $135^\circ$  we add or subtract  $180^\circ$  respectively. Restricting ourselves to the half circle, marked by the red arcs, ensures proper averaging of  $\Theta_{ij}^{BV}$  for low values of  $\tau$ , where photometric uncertainties dominate the slopes. A restriction to the full circle, or  $-90^\circ$  to  $90^\circ$ , would bias the slope towards  $0^\circ$  if the photometric errors are large compared to the true change of flux.

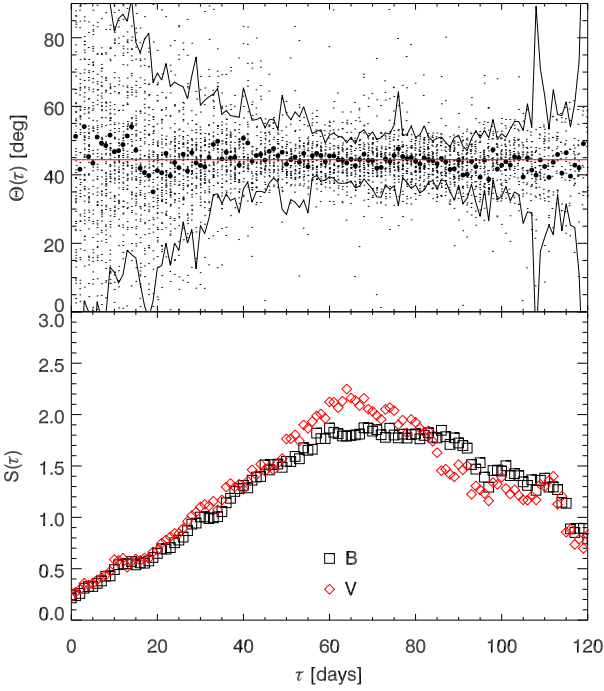


**Fig. 5.** Top: Small dots represent  $\Theta_{ij}^{BV}$  between all possible permutations of measurements  $i, j$  with  $\tau = |t_j - t_i|$ . Larger dots mark the averages inside a bin of one day with their uncertainty plotted as a continuous black line. The red straight line at  $44.4^\circ$  corresponds to the linear fit of all data  $\Gamma_{BV} = 0.979$ . Bottom: The structure function  $S$  of the variability; black boxes for  $B$ -band and red diamonds for  $V$ -band.

ensemble color variability of their quasars was not constant for all observed redshifts, showing rather blue slopes on short timescales of  $< 30$  days that turn to redder slopes on longer timescales.

Here we improve their approach in some aspects. Instead of using magnitudes, we make use of fluxes  $f_i$  directly. As pointed out by Kokubo et al. (2014) and references therein, fitting a straight line in magnitude–magnitude space (e.g. Sun et al. 2014) relies heavily on the contamination of the baseline flux by host galaxies and emission lines.

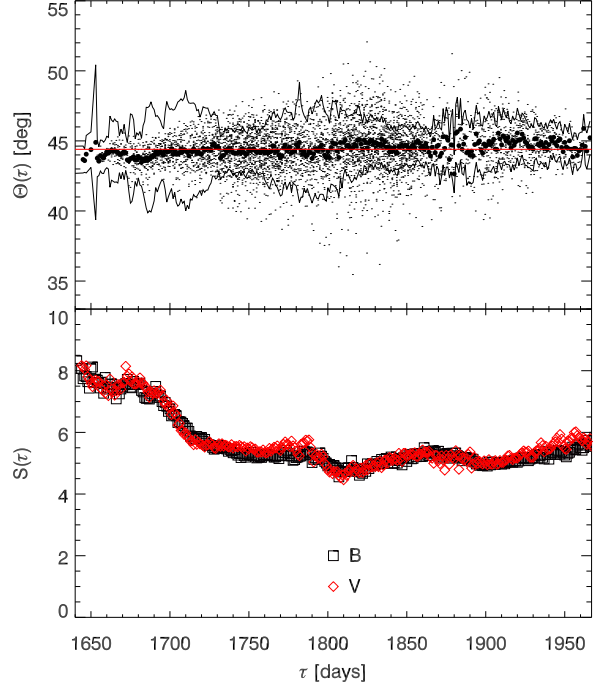


**Fig. 6.** Same as Fig. 5, here for the high values of  $\tau$  between the epochs of 2009 – 2010 and 2014 – 2015.

The color  $\Theta_{ij}^{BV}$  of an arbitrary flux variation in  $B$ - and  $V$ -band in the time interval  $\tau = |t_j - t_i|$  is computed using Equation 1. The geometry is explained in Fig. 4.

$$\Theta_{ij}^{BV}(\tau) = \arctan\left(\frac{f_B(t_j) - f_B(t_i)}{f_V(t_j) - f_V(t_i)}\right). \quad (1)$$

Like Sun et al. (2014), we restrict ourselves to the range of slopes  $-45^\circ < \Theta_{ij}^{BV} < 135^\circ$ . The slopes on the other half circle represent flux decreases and are rotated by  $180^\circ$  to their equivalent slopes for a flux increase. The offset of  $45^\circ$  is chosen to equally weigh cases of both bluer (i) when brighter ( $45^\circ < \Theta_{ij}^{BV} < 135^\circ$ ), and (ii) redder, when brighter ( $-45^\circ < \Theta_{ij}^{BV} < 45^\circ$ ), slopes in the averaging process. The angle of  $45^\circ$  represents no color change.

Our photometric measurements in all observed epochs offer  $\Theta_{ij}^{BV}$  for many combinations of  $t_i$  and  $t_j$ , with the lowest sampling interval of  $\tau = 1$  day. It is useful to average all  $\Theta_{ij}^{BV}$  inside bins with this size. The average of these bins is described by

$$\overline{\Theta}^{BV}(\tau) = \frac{1}{N} \sum_{ij} \Theta_{ij}^{BV}(\tau). \quad (2)$$

The results of this approach for the  $B$ - and  $V$ -band fluxes are shown in Fig. 5, together with the structure function  $S(\tau)$ , as defined by Equation 3. The latter is an indicator of the strength of the variability on a specific time scale  $\tau$ . The black solid lines enclose the average photometric uncertainty of each  $\tau$  bin.

$$S(\tau) = \sqrt{\frac{1}{N} \sum_{ij} (f_V(t_j) - f_V(t_i))^2}. \quad (3)$$

Analyzing photometric fluxes with large uncertainties  $\sigma_i, \sigma_j$ , compared to the difference in fluxes with  $|f_v(t_j) - f_v(t_i)| < \sqrt{\sigma_i^2 + \sigma_j^2}$ , can cause a bias on  $\Theta_{ij}$ . We assume a case of flux that is constant except for noise that is described by different photometric uncertainties for  $B$ - and  $V$ -band with  $\sigma_{fB} \gg \sigma_{fV}$ . Then, referring to the sketch in Fig. 4, we have  $\Delta f_B \gg \Delta f_V$  for samples of measurements drawn from these distributions. As a result, we obtain  $\Theta(\tau) \approx 90^\circ$ .

The structure function  $S(\tau)$  for the short timescales in Fig. 5 shows that for  $\tau < 20$  days the variations are still on the order of typical photometric errors. As a consequence, the distribution of  $\Theta_{ij}^{BV}$  is very broad in this region. The shape of the structure function is very similar for both bands with a slightly larger variation in amplitudes around 60 days for the  $V$ -band. For comparison purposes, we plot the previous linear fit result of  $\Gamma_{BV} = 0.979$  as solid red line. In this early epoch, the majority of slopes  $\overline{\Theta}^{BV}(\tau)$  is about  $3^\circ$  higher than the linear approximation but with only low significance and large scatter. From 20 to 90 days, the scatter decreases and the average cannot be distinguished from the linear fit. A potential contribution of  $\sim 5\%$  H $\beta$  at 25 days (Pozo Nuñez et al. 2012) may introduce additional flux to the  $V$ -band and shifts the slope downward in this region. However, there is no significant trace of this effect. After 90 days, the number of data points in the  $\tau$  bins decreases naturally, causing larger scatter and a minimally lower average slope of  $42^\circ$ . In summary, the plot reveals no clear difference in  $\overline{\Theta}^{BV}$  on timescales  $\tau$  within a single observation epoch of 3C 120.

In Figure 6, we restrict the plot to  $1640 < \tau < 1960$ , so that all  $\Theta_{ij}^{BV}$  have one data point in our early epoch of 2009 – 2010 and one in the late epoch of 2014 – 2015. In total, all angles  $\overline{\Theta}^{BV}$  are consistent with our linear fit result, taking the photometric uncertainties into consideration. Within the errors, there appears a positive slope from  $44^\circ$  to  $45^\circ$  for the considered range of  $\tau$ . This is, however, consistent with a potential host flux offset between the two epochs that originates from different PSFs as explained in Section 3.1.

#### 4. Discussion and conclusions

Our results show a highly linear evolution of  $B$  versus  $V$  fluxes for 3C 120 on all timescales – from days to several years. Additionally, the color is highly constant, despite the AGN undergoing a strong increase of 1.4 mag in flux over a duration of five years.

Calculating their time dependent colors  $\theta(\tau)$  in magnitude–magnitude space, Sun et al. (2014) report a significant change of color for  $g$ - and  $r$ -band data of a large SDSS quasar sample. The colors change from short timescale (small amplitude) blue colors to long timescale (large amplitude) red colors. Considering a total observed flux  $f(t) = f_{\text{Host}} + f_{\text{AGN}}(t)$ , composed of constant host galaxy component and variable AGN, the difference in magnitude space is

$$\Delta m_{ij}(\tau) = 2.5 \log \left( \frac{f_{\text{AGN}}(t_j) + f_{\text{Host}}}{f_{\text{AGN}}(t_i) + f_{\text{Host}}} \right). \quad (4)$$

This means that a constant host causes a reduction in the observed magnitude difference. Because the host galaxy SED is red, compared to that of the AGN, the magnitude difference will be reduced more for the red  $\Delta m_r(\tau)$  compared to the blue  $\Delta m_g(\tau)$  and therefore  $\theta(\tau) = \arctan(\Delta m_r(\tau)/\Delta m_g(\tau))$  turns to artificially

blue colors. Since the structure function of the SDSS quasars rises towards long timescales (Sun et al. 2014), we simultaneously observe large amplitudes of flux variations. Because the host galaxy contribution is reduced in such cases,  $\theta(\tau)$  will be of a redder color. In our flux–flux approach, however, this issue is completely avoided. Therefore, we suggest that the luminosity and time-dependent color variability observed by Sun et al. is an artifact of data analysis in magnitudes instead of fluxes.

The intrinsic brightness change of any astronomical object may be caused by a change in the area and/or the temperature  $T$  of the emitting surface. While an increase in area would simply cause a constant color, the temperature change always has a degree of curvature. Only in the Rayleigh-Jeans approximation is the flux again proportional to the temperature  $T$ . Using the blue side  $\lambda$  of the Johnson  $B$ -band in  $hc < \lambda k_B T$ , the temperature  $T$  must be higher than 36,000 K, because it is at the lower end of typical effective AD temperatures. The existence of a linear relationship between two (optical) fluxes shows that the variable component is hot enough to be approximated by Rayleigh Jeans.

Another mechanism for a brightness change is variable extinction. In this case, the extinction law influences the color of the varying component, with the bluer band usually more affected than the red band. As a result, extinction can provide a different color slope than a temperature fluctuation in the AD. However, extinction variations resulting from dust clouds that move into the line of sight are random events and should occur with diverse amplitude and timescales. Because they are independent of the variations in the AD with different its color, non-linear behavior of the total fluxes should then be observed in individual objects. Averaging a large sample of AGN flux variations, such random disturbances of the slope in the flux–flux diagrams will be washed out.

Our results are consistent with variations that stem from temperature changes in the AD, where the  $B$ - and  $V$ -bands are placed in the Rayleigh-Jeans tail of the thermal emission. There is no evidence for a short timescale, bluer color variation that may be caused by variable extinction in the line of sight.

In summary, our finding makes a good case for the use of the rest-frame optical FVG method on different timescales of low luminosity AGN. To further confirm this result, more longterm observations of varying Seyferts (and also quasars) with high photometric precision and dense (daily) temporal sampling will be required.

*Acknowledgements.* This research made use of the NASA/IPAC Extragalactic Database (NED) which is operated by the Jet Propulsion Laboratory, California Institute of Technology, under contract with the National Aeronautics and Space Administration (NASA). This publication is supported as a project of the Nordrhein-Westfälische Akademie der Wissenschaften und der Künste, in the framework of the academy program of the Federal Republic of Germany and the state of Nordrhein-Westfalen. This work is supported by the DFG Program (HA 3555/12-1). The observations on Cerro Armazones benefited from the support of guardians, Hector Labra, Gerardo Pino, Roberto Munoz, and Francisco Araya. We thank the referee, Ian Glass, for his helpful comments and careful review of the manuscript.

#### References

- Choloniewski, J. 1981, *Acta Astron.*, 31, 293
- Giveon, U., Maoz, D., Kaspi, S., Netzer, H., & Smith, P. S. 1999, *MNRAS*, 306, 637
- Kabath, P., Erikson, A., Rauer, H., et al. 2009, *A&A*, 506, 569
- Kokubo, M., Morokuma, T., Minezaki, T., et al. 2014, *ApJ*, 783, 46
- Meusinger, H., Hinze, A., & de Hoon, A. 2011, *A&A*, 525, A37
- Paltani, S. & Walter, R. 1996, *A&A*, 312, 55
- Pozo Nuñez, F., Ramolla, M., Westhues, C., et al. 2012, *A&A*, 545, A84
- Sakata, Y., Minezaki, T., Yoshii, Y., et al. 2010, *ApJ*, 711, 461

Sakata, Y., Morokuma, T., Minezaki, T., et al. 2011, ApJ, 731, 50  
 Schlafly, E. F. & Finkbeiner, D. P. 2011, ApJ, 737, 103  
 Sun, Y.-H., Wang, J.-X., Chen, X.-Y., & Zheng, Z.-Y. 2014, ApJ, 792, 54  
 Wamsteker, W., Rodriguez-Pascual, P., Wills, B. J., et al. 1990, ApJ, 354, 446  
 Webb, W. & Malkan, M. 2000, ApJ, 540, 652  
 Wilhite, B. C., Vanden Berk, D. E., Kron, R. G., et al. 2005, ApJ, 633, 638  
 Winkler, H. 1997, MNRAS, 292, 273  
 Winkler, H., Glass, I. S., van Wyk, F., et al. 1992, MNRAS, 257, 659

## Appendix A: Measured fluxes

**Table A.1.** Galactic foreground extinction corrected *B*-band fluxes from 2009 until 2015.

MJD	Flux	Error
days		mJy
55110.237	5.55421	0.105191
55111.234	5.8784	0.131488
55114.225	6.18674	0.111323
55115.223	6.09283	0.077608
55121.283	6.58088	0.132027
55123.203	6.37179	0.0947509
55124.209	6.5088	0.0957203
55125.209	6.49741	0.103942
55126.209	6.67802	0.126342
55127.264	6.39158	0.103038
55130.204	6.61423	0.0713771
55131.166	6.67221	0.110278
55132.208	6.55387	0.075334
55133.260	6.45186	0.0950582
55134.166	6.59332	0.0966424
55135.172	6.61771	0.114972
55136.209	6.96171	0.0903407
55137.175	7.07786	0.136614
55138.209	6.69046	0.158005
55139.218	7.12651	0.196419
55140.175	7.24073	0.196107
55141.175	6.96943	0.124644
55144.185	7.27056	0.118578
55146.175	6.874	0.0758508
55147.153	6.99352	0.121185
55148.216	6.89657	0.112869
55149.175	6.71507	0.0817101
55151.222	6.71472	0.136257
55153.145	6.84699	0.175694
55154.217	7.11164	0.142083
55156.181	7.02015	0.15446
55157.226	7.11348	0.171963
55158.164	7.42939	0.135409
55159.148	7.14331	0.085071
55160.268	7.41794	0.0926098
55161.144	7.36146	0.0904423
55162.188	7.12791	0.0774404
55163.262	7.22946	0.0724561
55164.148	7.12385	0.148103
55165.159	6.99121	0.065618
55166.200	7.24529	0.206256
55167.177	7.50535	0.127324

Table A.1 continued.

MJD	Flux	Error
55168.226	7.3375	0.197946
55181.213	7.32589	0.179363
55200.209	5.91065	0.101208
55201.179	5.57005	0.116409
55203.179	5.64471	0.194746
55204.216	5.37734	0.088279
55205.160	5.50883	0.0735336
55206.194	5.67506	0.0920804
55207.180	5.48779	0.0972899
55208.188	5.34417	0.118273
55209.185	5.35524	0.0988943
55210.200	5.44533	0.0826862
55212.181	5.41264	0.095357
55213.176	5.27572	0.0994904
55214.169	5.28162	0.0990277
55215.171	5.59415	0.107598
55216.185	5.40936	0.0881853
55217.145	5.6395	0.0854541
55218.158	5.48408	0.0979306
55219.161	5.70425	0.164234
55220.156	5.72685	0.125466
55221.153	5.8559	0.149499
55222.168	5.64563	0.134439
55223.128	5.92687	0.175566
55224.146	5.63153	0.125795
55225.142	5.97617	0.152117
55226.138	5.56186	0.13634
55228.152	5.43482	0.105249
55230.126	5.4637	0.10911
55231.127	5.70627	0.120521
55232.122	5.56605	0.124716
55236.111	5.50081	0.0723353
55238.111	5.70972	0.108597
55240.117	5.85487	0.10974
55241.081	6.02139	0.122924
55242.096	6.15323	0.0706417
55243.097	6.16286	0.101422
55244.087	6.26022	0.104736
55245.096	6.31632	0.0806359
55251.089	6.15306	0.107161
55254.081	6.05505	0.123017
56895.368	14.3804	1.04936
56897.366	14.1336	0.983937
56898.358	13.9633	0.147968
56899.358	13.7959	0.109101
56900.385	13.7324	0.226593
56903.344	13.3408	0.194499
56906.327	13.2489	0.976908
56907.343	13.1597	0.291964
56908.330	12.9185	0.220106
56909.325	12.7856	0.204544
56910.333	12.5424	0.262686
56911.312	12.2846	0.206587
56912.377	12.3907	0.266982
56920.377	12.3876	0.521437
56925.375	12.4381	1.49668
56926.373	12.1945	0.0961339

Table A.1 continued.

MJD	Flux	Error
56927.369	12.2455	1.18698
56928.367	12.3288	1.43678
56929.364	11.9162	1.7241
56930.361	11.7529	0.864746
56936.336	11.5692	0.10415
56937.335	11.29	0.0942527
56938.334	11.5188	0.268483
56939.334	11.5381	0.133113
56941.330	11.4562	0.576352
56943.325	11.5018	0.283021
56944.352	11.5507	0.11299
56946.374	11.6383	0.596045
56950.347	11.3615	0.0897234
56953.332	11.2265	0.121999
56956.323	10.9593	0.181796
56957.321	10.8346	0.332822
56958.321	11.0549	0.0997387
56959.313	11.1725	0.0734273
56960.311	10.9795	0.125564
56961.314	10.8968	0.120839
56964.273	10.665	0.0736191
56965.272	10.496	0.084032
56966.310	10.913	0.103403
56967.265	10.5722	0.156577
56968.306	10.2267	0.0856314
56969.261	10.5487	0.157831
56970.352	10.391	0.472495
56972.202	10.3721	0.148061
56973.287	10.1588	0.0703249
56974.284	10.1296	0.0993075
56975.258	10.2233	0.112217
56978.251	9.95252	0.0759752
56979.248	10.129	0.0708522
56980.246	10.3133	0.0943685
56981.243	10.3805	0.0763472
56982.240	9.92794	0.066818
56983.237	10.3451	0.0996063
56984.235	10.098	0.130562
56985.231	10.0103	0.0832779
56986.222	10.3187	0.0663072
56987.215	10.0418	0.095233
56988.211	9.94455	0.0923461
56989.211	9.98914	0.0576447
56990.230	10.1267	0.0918454
56991.199	10.2779	0.0700807
56994.243	10.6593	0.083241
56999.226	10.3593	0.109408
57000.196	10.9499	0.13015
57003.220	11.1454	0.090543
57005.216	11.1176	0.114169
57006.198	11.3441	0.0799838
57008.191	11.2517	0.069811
57009.205	11.0519	0.0910484
57010.192	10.8618	0.0919861
57011.188	10.946	0.0958581
57032.126	10.9831	0.268319
57035.126	11.7138	0.496919

Table A.1 continued.

MJD	Flux	Error
57038.123	11.7465	0.169581
57040.123	11.9359	0.102771
57041.122	11.9438	0.278621
57042.122	11.8676	0.310776
57047.059	12.2454	0.174759
57049.023	12.3322	0.15833
57050.022	12.5201	0.336703
57054.020	12.6104	0.374115
57056.067	12.4112	0.161701
57057.020	12.3306	0.171476
57058.020	12.1477	0.15279
57059.019	12.1763	0.122279
57060.019	11.9898	0.11905
57065.016	11.8339	0.208689
57066.016	11.8045	0.104941
57067.052	11.8566	0.0844698
57068.014	12.0699	0.114009
57069.014	11.9332	0.14584
57070.013	12.1462	0.155033
57071.013	12.0355	0.106119
57074.011	12.0657	0.180716
57075.010	11.6865	0.129328
57076.010	11.7541	0.144578
57077.009	11.861	0.11675
57078.008	11.6374	0.143872
57080.008	12.1926	0.310672
57081.007	11.6933	0.112834
57082.006	11.6342	0.160317
57083.005	12.0345	0.216004
57084.004	11.8517	0.231508
57085.004	11.7921	0.172509
57088.002	11.8821	0.148556
57089.002	11.9226	0.112329
57092.004	11.7295	0.147702
57093.997	11.8236	0.117837

**Table A.2.** Galactic foreground extinction corrected V-band fluxes from 2009 until 2015.

MJD	Flux	Error
days		mJy
55110.283	7.80492	0.107975
55111.280	8.13988	0.122128
55112.281	8.16902	0.185274
55113.274	8.40669	0.129154
55114.271	8.38676	0.107963
55115.269	8.48413	0.0902408
55121.329	8.71428	0.14702
55123.249	8.77489	0.128866
55124.255	8.97913	0.161263
55125.255	8.8118	0.174615
55126.255	9.05692	0.177551
55127.311	9.02664	0.112698
55130.215	8.83791	0.100329
55131.213	9.19359	0.173977
55132.161	8.79508	0.234881
55133.248	8.90878	0.0787138
55134.213	9.12944	0.109715
55135.219	8.99221	0.101696
55136.219	9.41409	0.0970858
55137.222	9.29944	0.19867
55139.208	9.44626	0.206467
55140.222	9.19151	0.238798
55141.221	9.24981	0.104757
55144.138	9.31401	0.1281
55146.223	9.49443	0.113287
55147.199	9.28943	0.139888
55148.227	9.46577	0.199261
55149.223	9.2952	0.201076
55151.211	9.37694	0.219707
55153.192	9.39334	0.233614
55154.228	9.35126	0.134791
55156.135	9.47155	0.291827
55157.216	9.87356	0.173444
55159.196	9.29006	0.147111
55160.280	9.58813	0.214793
55161.192	9.46201	0.161921
55162.139	9.57828	0.112009
55164.196	9.60405	0.103562
55165.207	9.32988	0.183195
55167.188	9.15643	0.211352
55168.214	9.41859	0.239692
55173.276	9.29753	0.176752
55174.295	9.36956	0.341082
55200.199	8.23195	0.100521
55201.189	8.28018	0.156595
55204.206	7.87946	0.124108
55205.170	7.85903	0.0732903
55206.184	7.8568	0.0907966
55207.190	7.9896	0.0916827
55208.178	7.82703	0.0989102
55209.196	7.72464	0.122169
55210.190	7.65428	0.133864
55212.170	7.53899	0.102164

**Table A.2 continued.**

MJD	Flux	Error
55213.186	7.56678	0.109318
55214.159	7.698 0	.152955
55215.181	7.71733	0.0871391
55216.174	7.81947	0.0996844
55217.155	7.99646	0.159476
55218.148	7.80512	0.105828
55219.171	7.79658	0.0913465
55220.146	7.95024	0.146176
55221.164	8.0759	0.174263
55222.158	7.65141	0.107348
55223.138	8.10472	0.157151
55224.136	7.94129	0.148864
55225.153	7.72148	0.328673
55226.128	7.46477	0.150035
55228.142	7.56282	0.140573
55230.116	7.89702	0.116355
55231.137	7.90614	0.0739646
55232.112	7.79313	0.0957212
55233.130	7.87441	0.156332
55236.101	7.99585	0.114276
55238.101	7.99872	0.119167
55240.107	8.27189	0.130001
55241.091	8.37387	0.0684091
55242.085	8.46378	0.0811344
55243.107	8.46584	0.1109
55244.077	8.60484	0.0984047
55245.107	8.61162	0.10168
55246.096	8.53311	0.112621
55250.085	8.53457	0.111314
55252.090	8.33699	0.131954
55254.071	8.37249	0.106794
56898.378	16.6557	0.186138
56900.322	16.1771	0.120272
56902.367	15.5529	0.254201
56910.310	15.0494	0.238098
56911.354	14.5983	0.191545
56920.261	14.7768	0.112215
56927.240	14.9211	0.186894
56928.240	14.6891	0.156857
56929.240	14.4583	0.157344
56930.230	14.2573	0.200672
56931.262	14.2388	0.121795
56932.304	14.1808	0.155984
56936.268	13.9515	0.220356
56937.268	13.8814	0.177064
56938.323	13.8499	0.301957
56941.267	14.0377	0.302282
56942.268	14.3559	0.294361
56943.261	13.8518	0.218258
56944.261	14.0379	0.226156
56949.247	14.2412	0.20211
56950.210	13.5852	0.169376
56951.199	13.8724	0.104292
56951.308	13.6163	0.242234
56953.227	13.3842	0.155249
56955.206	13.2942	0.103009
56956.206	13.4105	0.140081

Table A.2 continued.

MJD	Flux	Error
56957.206	13.3262	0.122764
56958.342	13.2041	0.300121
56959.205	13.3902	0.108892
56960.206	13.2339	0.221935
56961.206	13.323	0.142973
56962.206	13.0426	0.14191
56963.220	13.288	0.11486
56964.205	13.1691	0.11433
56965.192	12.7974	0.180278
56966.192	13.0069	0.130979
56967.175	13.0466	0.172496
56968.175	12.5915	0.292129
56969.175	12.8817	0.28501
56972.175	12.6383	0.150737
56973.175	12.8066	0.183076
56974.174	12.6368	0.101455
56975.174	12.5512	0.160767
56976.184	12.8272	0.137709
56978.177	12.4271	0.117361
56979.175	12.4385	0.110956
56980.172	12.5612	0.125104
56981.169	12.4201	0.128426
56982.166	12.5571	0.112808
56983.163	12.5241	0.127495
56984.160	12.4284	0.0935889
56999.121	13.0574	0.232812
57013.083	13.0503	0.157684
56898.394	16.4276	0.155995
56899.395	16.5029	0.245028
56900.422	16.3084	0.292189
56903.380	15.8189	0.162293
56904.354	16.0975	0.481578
56906.363	15.5928	0.227986
56907.379	15.7337	0.342789
56908.366	15.6151	0.180709
56909.360	15.1909	0.30776
56910.369	15.0948	0.136874
56911.348	14.8637	0.152151
56959.379	13.4723	0.244766
56961.380	13.5448	0.18189
56964.338	13.268	0.095813
56965.338	12.9671	0.103183
56967.330	13.1403	0.127211
56969.326	12.7035	0.139011
56991.264	12.8366	0.0982572
57008.240	13.4449	0.0784246
57010.241	13.4736	0.106579
57011.237	13.5716	0.142467
57032.176	13.3936	0.154944
57035.177	13.5697	0.15817
57038.172	14.2091	0.192206
57047.108	14.6907	0.0955832
57050.073	14.9109	0.339064
57056.117	14.5971	0.267836
57057.070	14.5593	0.145233
57058.070	14.4118	0.0502472
57059.069	14.4694	0.130669

Table A.2 continued.

MJD	Flux	Error
57060.069	14.5013	0.132637
57065.069	14.4286	0.145172
57066.066	14.3239	0.101617
57068.065	14.4446	0.0949995
57069.064	14.5274	0.121463
57070.064	14.5247	0.0796847
57071.063	14.3549	0.0858158
57074.037	14.4823	0.16363
57077.034	14.0762	0.127564
57086.003	14.2022	0.133571
57091.003	14.2806	0.105551
57093.997	14.616	0.131274